

PACS numbers: 42.55.Rz; 42.70. Hj; 81.05.Je
DOI: 10.1070/QE2008v038n09ABEH013637

Neodymium-doped laser yttrium oxide ceramics

S.N. Bagayev, V.V. Osipov, M.G. Ivanov, V.I. Solomonov, V.V. Platonov, A.N. Orlov, A.V. Rasuleva, V.V. Ivanov, A.S. Kaigorodov, V.R. Khrustov, S.M. Vatnik, I.A. Vedin, A.P. Maiorov, E.V. Pestryakov, A.V. Shestakov, A.V. Salkov

***Abstract*. We studied mechanical, optical, and lasing parameters of neodymium-doped yttrium oxide ceramics synthesised by using a new technology involving the laser synthesis of nanopowders and their magnetic pulsed compaction. The fracture toughness of ceramics to cracks and its microhardness were measured to be $K_{IC} = 0.9 - 1.4$ MPa m$^{1/2}$ and $H_v = 11.8$ GPa, respectively. Ceramic samples sintered in the temperature range from 1550 to 2050 °C have the porosity $(1 - 150) \times 10^{-4}$ % and the optical loss coefficient $\alpha_{1.07} = 0.03 - 2.1$ cm^{-1} at a wavelength of 1.07 μm. It is shown that such porosity does not affect the optical loss coefficient of light. Lasing at ~ 1.079 μm with a slope efficiency of 15 % was obtained in a 1.1-mm-thick sample pumped by laser diodes.**

Keywords: *yttrium oxide, laser synthesis of powders, magnetic pulsed compaction, ceramics, absorption, lasing.*

1. Introduction

In recent years extensive investigations are performed in the field of synthesis of new materials by using nanotechnologies. One of the important directions is the manufacturing of optical ceramics for active media of solid-state lasers. The advantages of laser ceramics over single crystals are obvious. These are the possibility of manufacturing multilayer elements of size exceeding the size of single crystals, a higher concentration of active centres, a shorter time and a lower cost of manufacturing [1, 2]. Thus, the development of technology for synthesis of laser ceramics will solve the problem of manufacturing low-cost and compact technological lasers and high-power laser systems.

The main stages in the synthesis of optical ceramics are: (i) the synthesis of weakly agglomerated nanopowders of the specified composition; (ii) preparation of high-density samples (compacts) from them; and (iii) sintering of porous-free ceramics from compacts. The technological conditions for each of the next stages depend on the quality of the product obtained at the previous stage.

The most intricate problem is the synthesis of nanopowders of the specified composition [3]. This problem was solved in papers [4 – 9] and many others by the method of deposition of an yttrium oxide precursor from the aqueous solution of yttrium salts. The precursor was transformed to an yttrium oxide nanopowder after the proper thermal treatment. However, the choice of the method for precursor synthesis to obtain weakly agglomerated nanopowders is a complicated problem, which requires an individual approach for each material. The authors of [1, 2, 10] proposed a more universal method for synthesis of ceramics of a complex composition by mixing mechanically nano- and submicron powders of different oxides. In this case, however, sintering is performed simultaneously with solid-phase synthesis, which considerably complicates the possibility of obtaining transparent ceramics.

Compacts are prepared from nanopowders by using uniaxial and isostatic compaction [3, 4] and slip casting with the addition of surfactants (binders), which are specific for each of the powder types [1, 2, 10]. In this case, samples of density achieving more than 50 % of the density of corresponding crystals are produced. The presence of voids in compacts is favourable to the formation of pores in ceramics being sintered [11]. The problem of sintering of porous-free ceramics is solved by adding various compounds (chemical compounds of thorium [3, 4], silicon [1, 2, 10] or magnesium [12]) into nanopowders, which improve sintering and prevent the growth of crystallites during this process. In some cases, these additions improve the quality of ceramics. In particular, the addition of silicon oxide [1, 2] improves the solubility of neodymium in yttrium oxide. However, the choice of optimal additions and their concentration is also a quite complicated problem.

In this paper, we present the results of the study of laser ceramics synthesised by the method different from that used in [1, 4, 6]. The technology proposed in our paper involves two new processes: the laser synthesis [13 – 18] of weakly agglomerated surfactant powders of a complex composition with a narrow size distribution of particles within 2 – 40 nm, the average size of particles being 10 – 15 nm, and pulsed

S.N. Bagayev, S.M. Vatnik, I.A. Vedin, A.P. Maiorov, E.V. Pestryakov Institute of Laser Physics, Siberian Branch, Russian Academy of Sciences, prosp. Akad. Lavrent'eva 13/3, 630090 Novosibirsk, Russia; e-mail: vatnik@laser.nsc.ru;
V.V. Osipov, M.G. Ivanov, V.I. Solomonov, V.V. Platonov, A.N. Orlov, A.V. Rasuleva, V.V. Ivanov, A.S. Kaigorodov, V.R. Khrustov Institute of Electrophysics, Ural Branch, Russian Academy of Sciences, ul. Amundsena 106, 620016 Ekaterinburg, Russia; e-mail: plasma@iep.uran.ru;
A.V. Shestakov ELS-94 Limited Liability Company, Research and Production Center, ul. Vvedenskogo 3, 117342 Moscow, Russia;
A.V. Salkov Elakom Limited Liability Company, ul. Vvedenskogo 3, 117342 Moscow, Russia

Received 18 May 2007; revision received 24 March 2008
Kvantovaya Elektronika **38** (9) 840 – 844 (2008)
Translated by M.N. Sapozhnikov

compaction [19] of these nanopowders at pressure amplitudes up to 1.5 GPa, which allows us to fabricate rigid homogeneous compacts of density up to 0.7 of the crystal density without using binding additions.

2. Laser synthesis of nanopowders

Nanopowders were prepared by using a 10.6-μm repetitively pulsed LAERT CO_2 laser developed at the Institute of Electrophysics, Ural Branch, RAS [20]. The target evaporation regime could be controlled by varying the main parameters of the laser radiation. Nanopowders were synthesised by using 10–11-kW, 250-μs pulses emitted at a repetition rate of 500 Hz. The average radiation power was between 600 and 800 W, the consumed power was 8 kW, and the laser beam aperture was 35×35 mm.

Targets for evaporation were prepared of commercial Y_2O_3 and Nd_2O_3 powders with grains of size 5–10 μm and purity 99.99 %. After the laser evaporation of targets, nanopowders of yttrium oxide with the molar concentration of neodymium oxide $C_{Nd} = 0\,\%$, 1 %, and 3 % were obtained. The efficiency of production of nanopowders was virtually independent of the target composition and amounted to 24 g h^{-1} for the laser energy consumption 90 kJ g^{-1}.

Electron microscope analysis showed that nanopowder particles are weakly agglomerated and form two fractions. The main fraction (with the mass concentration 93 %–97 %) consists of spherical particles of size 2–40 nm (the average size was 10 nm). The second fraction consists of spherical particles of size 0.2–2 μm, which appear due to the splashing out of liquid from the laser crater. The second fraction also contains shapeless particles of size 1–100 μm, which represent the 'fragments' of the laser crater on the target formed during the solidification of a liquid melt pool in the crater (straight tracks appearing in the shadow photographs of a laser plume within 1 ms after the laser pulse end demonstrate flying apart large particles [21]). The main fraction can be separated from large particles by the sedimentation of the powder in isopropanol.

X-ray diffraction analysis performed by using a DRON-4 diffractometer showed that the particles of the main fraction of the powder, as in [22], had the monoclinic γ-Y_2O_3 phase with parameters dependent on the molar concentration of neodymium oxide. For $C_{Nd} \approx 1\,\%$, the lattice constants were $a = 0.13922 \pm 0.00005$ nm, $b = 0.3940 \pm 0.0002$ nm, $c = 0.8615 \pm 0.0004$ nm and the angle was $\beta = 99.93^\circ \pm 0.08^\circ$; for $C_{Nd} = 3\,\%$, the lattice constants were $a = 0.14690 \pm 0.0005$ nm, $b = 0.3960 \pm 0.0002$ nm, $c = 0.9066 \pm 0.0004$ nm and the angle was $\beta = 110.50^\circ \pm 0.08^\circ$. The change in the parameters clearly demonstrates that neodymium ions have entered into the γ-Y_2O_3 crystal lattice.

3. Preparation of compacts from powders and sintering of ceramics

Nanopowders were compacted by uniaxial magnetic pulsed compaction [19]. A nanopowder filled in a press mould was degassed down to the residual pressure ~ 1 Pa and then pressed at pressures from 1.5 to 0.5 GPa. The compacts obtained in this way (homogeneous discs of diameter 15 or 32 mm and thickness 0.5–2.5 mm) had the density from 4.00 to 2.75 g cm^{-3} at pressures 1.5 and 0.5 GPa, respectively, which corresponded to 72 % and 50 % of the density of the crystal in the monoclinic modification. To eliminate organic inclusions and relaxation of residual mechanical stresses, the compacts were additionally annealed in air for 1–5 h at temperatures 1000–1300 °C and then were sintered in vacuum furnaces.

The sintering parameters were varied in a broad range: the sintering temperature was $T_s = 1550 - 2050$ °C, sintering time was $t_s = 1 - 30$ h, and the rate of temperature rise was $V_T = 0.75$ and 5.0 K min^{-1} (the heating curve with $V_T = 0.75$ K min^{-1} corresponded to the linear shrinkage of compacts with $C_{Nd} = 3\,\%$). All the ceramic samples were transparent after annealing, grinding, and polishing (Fig. 1), while neodymium-doped samples had blue colour with a weak lilac tint. They were used to fabricate plane–parallel plates of thickness 0.5–2.5 mm.

Figure 1. Photograph of a Nd^{3+}: Y_2O_3 ceramic sample with molar concentration of neodymium oxide of 1 % [the inscription means IEP, UB, RAS (Institute of Electrophysics, Ural Branch, Russian Academy of Sciences].

X-ray diffraction analysis performed by using a DRON-4M diffractometer showed that crystallites in ceramics represent the solid solution of neodymium in cubic yttrium oxide [23]. The entering of neodymium into the crystal lattice is confirmed by the increase in the lattice constant a with increasing the neodymium oxide content: $a = 1.0603$, 1.0606, and 1.0618 ± 0.0005 nm for $C_{Nd} \approx 0\,\%$, 1 %, and 3 %, respectively.

The density of ceramics at the sintering temperature $T_s \geqslant 1750$ °C achieved almost 100 % of the tabulated density of a Y_2O_3 crystal in the cubic modification ($\rho_{theor} = 5.04$ g cm^{-3} [24]) with the molar concentration of neodymium oxide 1 %.

Electron and optical microscope studies showed that ceramics consists of close-packed crystallites with the average size d increasing with the sintering temperature and time: $d = 0.5 - 1$, 5–10, 30–50, and 100–300 μm for $T_s = 1523 - 1550$, 1670–1750, 1850–1900, and 2050 °C, respectively. Other conditions being the same, the crystallite size decreases with increasing the neodymium content. The thickness of the interface between crystallites is independent of the crystallite size, but changes from 0.98 to 2.5 nm depending on the sintering conditions [24].

The microhardness H_v under the load of 0.5 N and fracture toughness K_{IC} were measured with a Nanotest 600

device by using a diamond Vickers pyramid. Ceramics with crystallites of the minimal size had the best mechanical parameters. In particular, ceramics with $d = 0.5 - 1$ μm had the fracture toughness $K_{IC} = 4.2$ MPa m$^{1/2}$ and the microhardness $H_v = 12.8$ GPa under the load of 0.5 N. However, this ceramics has a comparatively low transparency. As the size of crystallites increases from 0.5 to 5 μm, the transparency of ceramics increases but its mechanical parameters decrease considerably (down to $K_{IC} = 0.9 - 1.4$ MPa m$^{1/2}$ and $H_v = 11.8$ GPa). These parameters are virtually stabilised in the range of crystallite sizes from 5 to 50 μm.

Thus, homogeneous compacts with the density exceeding 0.7 of the crystal density are produced by magnetic pulsed compaction of $Nd^{3+}:Y_2O_3$ nanopowders. By sintering the samples in a vacuum furnace, we obtained transparent and mechanically rigid $Nd^{3+}:Y_2O_3$ ceramics with the sizes of crystallites and interface between them of the same order of magnitude as in the case of using additions restricting the growth of crystallites [1, 4, 6].

4. Optical properties of ceramics

Absorption spectra in the wavelength range from 400 to 1200 nm including the scattering of light by inhomogeneities were measured by using a spectral setup based on an MDR-23 monochromator. A radiation source in the 400–800-nm range was a DDS-30 lamp, and radiation was detected with a FEU-106 photomultiplier. In the range from 650 to 1200 nm, an OP-33-0.3 lamp and a FEU-62 photomultiplier were used. Sample surfaces were polished before measurements. The beam from a radiation source restricted by a rectangular aperture of size 4×6 mm was incident perpendicular to the polished surface of samples of thickness $h = 1 - 1.5$ mm. The optical loss coefficient of light by ceramics is described by the expression

$$\alpha(\lambda) = -\frac{1}{h} \ln \left[\frac{I(\lambda)}{I_0(\lambda)(1-R)^2} \right],$$

where $I_0(\lambda)$ and $I(\lambda)$ are the light intensities incident on and transmitted through a sample, respectively; $R = [n(\lambda) - 1]^2 \times [n(\lambda) + 1]^{-2}$ is the Fresnel reflectance of light from the surfaces of the sample; and $n(\lambda)$ is the refractive index of ceramics. We used in calculations the value $n = 1.91$ [25] at a wavelength of 1.07 μm [25]. The optical loss coefficient $\alpha_{1.07}$ of ceramics measured at this wavelength decreased, as a rule, with increasing the sintering temperature of ceramics, and its value varied from 0.03 to 2.1 cm^{-1} in different ceramic samples.

The absorption spectra of all ceramic samples exhibit the absorption bands of neodymium ions (Fig. 2), their intensity (at the same neodymium concentration) being invariable in compacts heated at the same rate but up to different sintering temperatures (from 1800 to 2050 °C). However, the parameters of the spectrum depend considerably on the heating rate of compacts up the sintering temperature. In particular, the absorption spectra of samples with the same neodymium concentration heated at the rates $V_T = 0.75$ K min^{-1} [curve (*1*) in Fig. 2] and $V_T = 5$ K min^{-1} [curve (*2*) in Fig. 2] are different. In the latter case, the intensity of absorption bands of neodymium and continuous absorption (especially in the region $\lambda \leqslant 600$ nm) is lower almost by half and, in addition, the intensities of the Stark components of

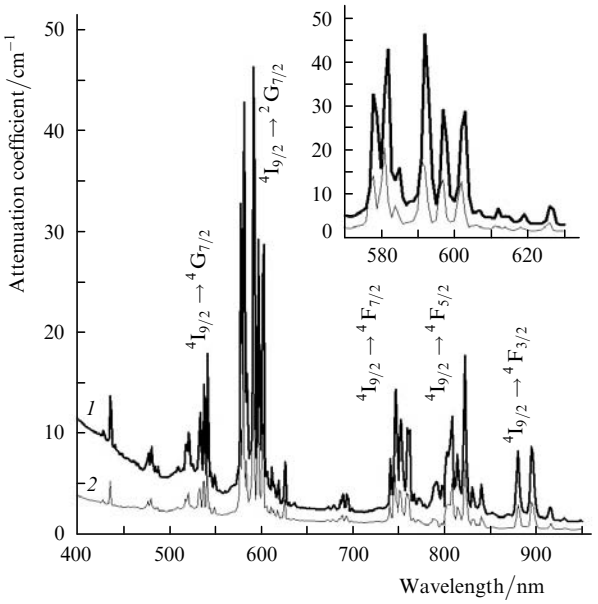

Figure 2. Absorption spectra of ceramic samples sintered at $T_s = 1900$ °C at the heating rates of samples $V_T = 0.75$ (*1*) and 5 K min^{-1} (*2*). The inset demonstrates the intensity redistribution of Stark components of the absorption band of neodymium ions in the region from 570 to 630 nm.

the absorption bands at the $^4I_{9/2} \rightarrow {}^2G_{7/2}$ transitions are redistributed (inset in Fig. 2). To elucidate the reasons for this behaviour of the absorption spectra, we analysed the content of defects in ceramics by using an OLYMPUS BX51TRF optical microscope.

The analysis showed that ceramics contains defects of two types – pores and inclusions. Quantitative measurements were performed by counting defects and their sizes in five and three regions of ceramic discs of diameters 32 and 15 mm, respectively. Measurements were performed in a volume with the 1×1-mm square cross section and height equal to the ceramics thickness. The volume concentration of defects of each type was defined as the ratio of the measured volume of defects to the region volume averaged over all regions.

Pores. Pores of diameters 0.5–3 μm in all samples were located predominantly on the boundaries of crystallites. Their volume concentration in different samples was from 1×10^{-4} % to 150×10^{-4} % depending on the sintering regime. The concentration noticeably decreases with decreasing the heating rate of compacts from 5 to 0.75 K min^{-1} and with increasing the sintering time. Other conditions being the same, the higher concentration of pores was measured in ceramics sintered from compacts with the lower initial density. In addition, in some samples the sites of size ~ 100 μm were found in which agglomerations of small pores were observed. These sites were formed by an organic dust consisting of flakes or filaments, which entered the sample at its preparation stage and was burnt out during sintering. The content of such pores in samples having the best porosity was $\sim 1 \times 10^{-4}$ %.

Inclusions. Inclusions of size 20–50 μm were detected only in samples sintered from a non-sedimented nanopowder, independently of compaction and sintering conditions. They are uniformly distributed in the ceramic volume and their volume concentration is approximately the

same for all samples and does not exceed 1×10^{-3} %. These inclusions are formed by large particles of the second fraction existing in the nanopowder, whereas spherical and shapeless particles smaller than 10 μm from the second fraction do not produce any visible defects.

A comparison of the results of optical measurements with the data of defect analysis showed that the optical loss coefficient $\alpha_{1.07}$ was almost independent of the volume concentration of pores in the range $(1 - 150) \times 10^{-4}$ %. Moreover, the change in the absorption spectrum shown in Fig. 2 does not correlate with the concentration of pores and inclusions. Therefore, the reason for the change in the absorption spectrum with changing the rate of heating compacts up to the sintering temperature requires a more detailed investigation.

Thus, optical measurements showed that the synthesised ceramics is transparent enough for obtaining lasing in it: the measured optical loss coefficient was as low as $\alpha_{1.07} = 0.03$ cm^{-1}. To synthesise ceramics not containing inclusions, the initial nanopowder should not contain shapeless particles exceeding 10 μm. The content of pores in ceramics decreases with decreasing the rate of heating compacts up to the sintering temperature and with increasing the sintering time.

5. Lasing

Continuous wave lasing was obtained in a 1.1-mm-thick ceramic sample with the optical loss coefficient $\alpha_{1.07} = 0.03$ cm^{-1}. Pumping was performed by three 2-W ATC-C-2000-200 laser diodes connected in parallel to a LDD-10 power supply. The diodes were tuned in a narrow spectral region near 807 nm by varying their temperature to achieve the maximum absorption of pump radiation in ceramics (about 20 %). The surfaces of a sample were polished to obtain the first smoothness class and were covered by an AR coating reflecting no more than 0.2 % at a wavelength of 1.08 μm.

The lasing parameters of ceramics were studied in a short optical cavity assembled for this purpose. The inset in Fig. 3 shows the experimental scheme. A dielectric coating with the reflectance 99.9 % at a wavelength of 1.079 μm and transmission 97 % at the pump wavelength deposited on one of the plane surfaces of a ceramic sample was used as a highly reflecting (HR) mirror. A convex mirror with the radius of curvature 80 mm and the reflectance 97 % at the laser wavelength was used as the output mirror of the cavity of length 1.6 mm. The pump radiation was focused by a lens on the mirror surface of the sample into a spot of diameter 150 μm corresponding to the size of the TEM_{00} mode of the cavity. The pump spot was scanned over the sample by moving the lens in the horizontal and vertical planes. The cavity was simultaneously tuned to obtain the maximum output power. The output and pump powers were measured with an Ophir L30A power meter with a cut-off filter made of a 0.5-mm-thick silicon plate.

Figure 3 presents the dependence of the output lasing power of the ceramic sample on the absorbed pump power. The linear approximation of the experimental data in the pump power range from 0.1 to 0.6 W is shown by the dashed straight line. A small deviation from the linear dependence at high pump powers can be caused by thermooptical distortions because no special thermal stabilisation of the sample was used. According to our measurements, the slope efficiency of lasing at a wavelength of 1.079 μm was 15 % and the total optical efficiency was 10 %.

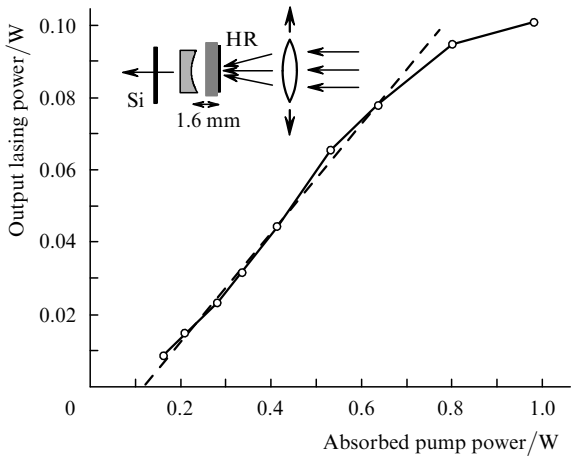

Figure 3. Dependence of the output lasing power of a ceramic sample on the absorbed pump power (the dashed straight line in the linear approximation). The inset shows the scheme of the experiment.

6. Conclusions

We have developed the technology for synthesis of optical $Nd^{3+}:Y_2O_3$ ceramics for active elements of solid-state lasers. The technology involves the preparation of finely divided nanopowders by laser synthesis, their magnetic pulsed compaction and sintering of compacts in vacuum furnaces without surfactant additions restricting the growth of crystallites.

This technology has been used to synthesise $Nd^{3+}:Y_2O_3$ ceramic samples with the fracture toughness $K_{IC} = 0.9-1.4$ MPa $m^{1/2}$, microhardness $H_v = 11.8$ GPa, porosity $(1 - 150) \times 10^{-4}$ %, and the optical loss coefficient of light $\alpha_{1.07} = 0.03 - 2.1$ cm^{-1} at a wavelength of 1.07 μm. It has been shown that $\alpha_{1.07}$ is independent of the volume content of pores in the range $(1 - 150) \times 10^{-4}$%. Continuous wave lasing has been obtained at 1.079 μm with a slope efficiency of 15% in a ceramic sample with $\alpha_{1.07} = 0.03$ cm^{-1}.

Acknowledgements. This work was supported by the program 'Femtosecond Optics and New Materials' of the Presidium of RAS and the Ural Branch, RAS.

References

1. Ikesue A., Kinoshita T., Kamata K., et al. *J. Am. Ceram. Soc.*, **78**, 1033 (1995).
2. Ikesue A., Aung Y.L., Taira T., et al. *Annu. Rev. Mater. Res.*, **36**, 397 (2006).
3. Gusev A.I., Rempel' A.A. *Nanokristallicheskie materialy* (Nanocrystal Materials) (Moscow: Fizmatlit, 2000).
4. Greskovich C., Chernoch J.P. *J. Appl. Phys.*, **44**, 4599 (1973).
5. Greskovich C., Wood K.N. *Am. Ceram. Soc. Bull.*, **52**, 473 (1973).
6. Lu J., Prabhu M., Ueda K., et al. *Jpn. J. Appl. Phys.*, **39**, 1048 (2000).
7. Lu J., Ueda K., Yagi H., et al. *J. Alloys Compounds*, **341**, 220 (2002).
8. Lu J., Murai T., Takaichi K., et al. *Jpn. J. Appl. Phys.*, **40**, 1277 (2001).
9. Kunar G.A., Lu J., Kaminskii A.A., et al. *IEEE J. Quantum Electron.*, **42**, 643 (2006).
10. Ikesue A., Furusato I., Kamata K., et al. *J. Am. Ceram. Soc.*, **78**, 225 (1995).
11. Slamovich E.B., Lange F.F. *J. Am. Ceram. Soc.*, **75**, 2498 (1992).

12. Jorgensen P.J., Westbrook J.H. *J. Am. Ceram. Soc.*, **47**, 332 (1964).
13. Osipov V.V., Kotov Yu.A., Ivanov M.G., et al. *Izv. Ross. Akad. Nauk, Ser. Fiz.*, **63**, 1968 (1999).
14. Kotov Yu.A., Osipov V.V., Ivanov M.G., et al. *Zh. Tekh. Fiz.*, **72**, 76 (2002).
15. Kotov Yu.A., Osipov V.V., Ivanov M.G., et al. *Rev. Adv. Mater. Sci.*, **5**, 171 (2003).
16. Kotov Yu.A., Osipov V.V., Samatov O.M., et al. *Zh. Tekh. Fiz.*, **74**, 72 (2004).
17. Kotov Yu.A., Osipov V.V., Ivanov M.G., et al. *Proc. SPIE Int. Soc. Opt. Eng.*, **6344**, 1 (2005).
18. Osipov V.V., Kotov Yu.A., Ivanov M.G., et al. *Laser Phys.*, **16**, 116 (2006).
19. Ivanov V.V., Paranin S.N., Vikhrev A.N., et al. *Materialovedenie*, **5**, 49 (1977).
20. Osipov V.V., Ivanov M.G., Lisenkov V.V., et al. *Kvantovaya Elektron.*, **32**, 253 (2002) [*Quantum Electron.*, **32**, 253 (2002)].
21. Osipov V.V., Solomonov V.I., Ivanov M.G., et al., in *Book of Abstracts Intern. Conf. on Advanced Laser Technol. ALT'06* (Brasov, Romania, 2006) p. 19.
22. Skandan G., Foster C.M., Frase H., et al. *Nanostruct. Mater.*, **1**, 313 (1992).
23. Kaigorodov A.S., Ivanov V.V., Khrustov V.R., et al. *J. Europ. Ceramic Soc.*, **27**, 1165 (2007).
24. Barabanenkov Yu.N., Ivanov V.V., Ivanov S.N., et al. *Zh. Eksp. Ter. Fiz.*, **129**, 131 (2006).
25. Kaminskii A.A. *Laser Crystals* (Berlin-Heidelberg-New York: Springer, 1981; Moscow: Nauka, 1975).